Ultrafast Dynamics of Phytochrome from the Cyanobacterium *Synechocystis*, Reconstituted with Phycocyanobilin and Phycoerythrobilin

Karsten Heyne,* Johannes Herbst,* Dietmar Stehlik,* Berta Esteban,† Tilman Lamparter,† Jon Hughes,‡ and Rolf Diller*

*Institut für Experimentalphysik and †Institut für Pflanzenphysiologie, Freie Universität Berlin, D-14195 Berlin, and ‡Pflanzenphysiologie, Zeughaus, D-35390 Giessen, Germany

ABSTRACT Femtosecond time-resolved transient absorption spectroscopy was employed to characterize for the first time the primary photoisomerization dynamics of a bacterial phytochrome system in the two thermally stable states of the photocycle. The 85-kDa phytochrome Cph1 from the cyanobacterium *Synechocystis* PCC 6803 expressed in *Escherichia coli* was reconstituted with phycocyanobilin (Cph1-PCB) and phycoerythrobilin (Cph1-PEB). The red-light-absorbing form Pr of Cph1-PCB shows an ~150 fs relaxation in the S_1 state after photoexcitation at 650 nm. The subsequent Z-E isomerization between rings C and D of the linear tetrapyrrole-chromophore is best described by a distribution of rate constants with the first moment at $(16\ \text{ps})^{-1}$. Excitation at 615 nm leads to a slightly broadened distribution. The reverse E-Z isomerization, starting from the far-red-absorbing form Pfr, is characterized by two shorter time constants of 0.54 and 3.2 ps. In the case of Cph1-PEB, double-bond isomerization does not take place, and the excited-state lifetime extends into the nanosecond regime. Besides a stimulated emission rise time between 40 and 150 fs, no fast relaxation processes are observed. This suggests that the chromophore-protein interaction along rings A, B, and C does not contribute much to the picosecond dynamics observed in Cph1-PCB but rather the region around ring D near the isomerizing $C_{15}{=}C_{16}$ double bond. The primary reaction dynamics of Cph1-PCB at ambient temperature is found to exhibit very similar features as those described for plant type A phytochrome, i.e., a relatively slow Pr, and a fast Pfr, photoreaction. This suggests that the initial reactions were established already before evolution of plant phytochromes began.

INTRODUCTION

Phytochromes are photochromic photoreceptors that were first discovered in plants where they control numerous photomorphogenetic processes such as development of the photosynthetic apparatus, shade avoidance, and the induction of flowering (Chory et al., 1996; Casal et al., 1998; Smith, 1999). Plant phytochromes consist of an ~120-kDa apoprotein with a covalently linked open-chain tetrapyrrole chromophore, usually phytochromobilin (PΦB). Concerning functional aspects the holoprotein can be divided into two parts, the N-terminal moiety containing the chromophore binding site and the elements for photoactivity and the C-terminal moiety, which is regarded as the module for dimerization and signal transduction (Quail et al., 1995). All phytochromes have two thermally stable forms, namely, the red-absorbing form Pr ($\lambda_{max} \approx 670$ nm) and the far-red-absorbing form Pfr ($\lambda_{max} \approx 730$ nm). Pr and Pfr are interconverted by photo-induced Z-E and E-Z isomerization reactions, respectively, around the chromophore $C_{15}{=}C_{16}$-methine bridge (Rüdiger et al., 1983; Thümmler and Rüdiger, 1983; Schaffner et al., 1990). The dynamics of the primary Pr and Pfr photoreactions of plant phytochrome A have been studied by transient absorption and time-resolved fluorescence spectroscopy. For the Pr→Pfr photoreaction, the formation of the first intermediate electronic ground state is described mostly by time constants between 10 and 60 ps (Holzwarth et al., 1984, 1992; Kandori et al., 1992; Savikhin et al., 1993; Andel et al., 1997; Rentsch et al., 1997; Bischoff et al., 2001; Müller and Holzwarth, Max-Planck-Institut für Strohlenchemie, Mülheim, personal communication), but shorter as well as longer time constants have also been reported (Holzwarth et al., 1984, 1992; Bischoff et al., 2001). In addition, very fast relaxation processes on the time scale of up to a few hundred femtoseconds have been found (Büchler et al., 1995; Bischoff et al., 2001; Müller and A. Holzwarth, Max-Planck-Institut für Strohlenchemie, Mülheim, personal communication). The reverse Pfr→Pr photoreaction is faster and is described as a biexponential process with ~0.4–0.6 and 2–3 ps time constants (Müller and Holzwarth, Max-Planck-Institut für Strohlenchemie, Mülheim, personal communication; Bischoff et al., 2001). The respective reaction products, Pfr and Pr, are formed on the millisecond time scale by thermally driven reactions via various intermediate states of the chromophore-protein complex. Although it seems clear that the process of signal transduction is initiated by the primary photoreactions of Pr and Pfr, respectively, only little is known about the mechanisms, e.g., protein conformational changes, that associate phytochrome photoconversion with physiological functions. This is partly due to the lack of a three-dimensional structural model of phytochrome on an atomic level.

Submitted July 13, 2001, and accepted for publication October 23, 2001.

Dr. Heyne's present address is Max-Born-Institut, Max-Born-Strasse 2A, D-12489, Berlin, Germany.

Address reprint requests to Dr. Rolf Diller, Institut für Experimentalphysik, Fachbereich Physik (WE 1), Arnimallee 14, D-14195 Berlin, Germany. Tel.: +49-30-8385-6107; Fax: +49-30-8385-6081; E-mail: diller@physik.fu-berlin.de.

0006-3495/02/02/1004/13 $2.00

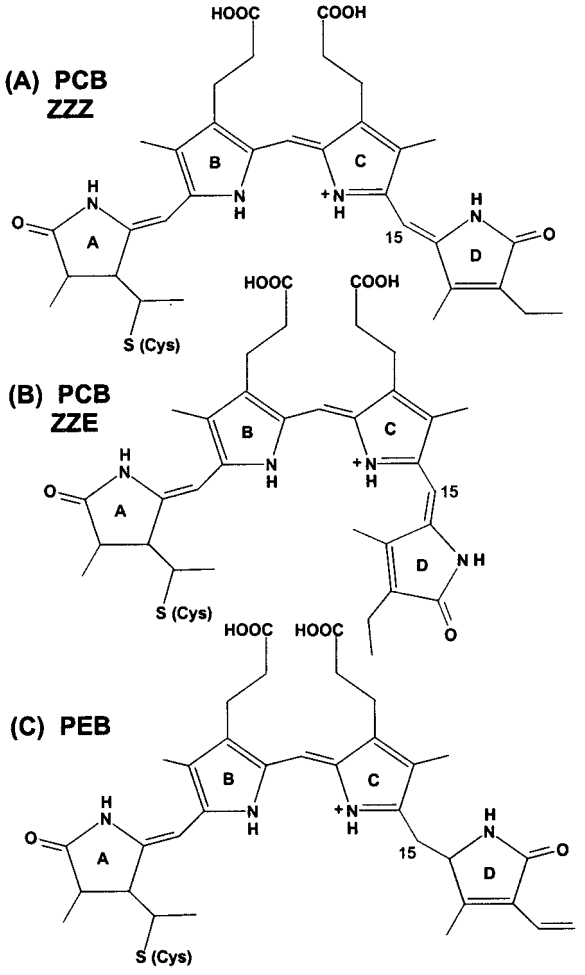

FIGURE 1 (*A* and *B*) Structure of phycocyanobilin (PCB) in ZZZ (*A*) and ZZE (*B*) configuration; (*C*) Structure of phycoerythrobilin (PEB). Shown are schematic views of potential chromophore structures when bound to the protein via a cysteine-residue at ring A.

The discovery of prokaryotic phytochromes and phytochrome-like proteins has shed new light on this group of photoreceptors. The diversity of phytochrome-homologous motifs is much greater than in the plant world, and it is generally accepted that plant phytochromes originate from prokaryotic predecessors. Among the prokaryotic phytochrome-like sequences, the 85-kDa phytochrome Cph1 from the cyanobacterium *Synechocystis* PCC 6803 is closely related to the plant phytochrome group. After expression in *Escherichia coli* (Hughes et al., 1997; Yeh et al., 1997; Lamparter et al., 1997), the apoprotein Cph1 can be assembled autocatalytically with phycocyanobilin (PCB), phycoerythrobilin (PEB) (Fig. 1), or PΦB to yield a functional chromoprotein. In the natural host *Synechocystis*, Cph1 is associated with PCB (Cph1-PCB) (Hübschmann et al., 2001). Compared with PΦB, PCB lacks one double bond in the C2 side chain in ring D. Accordingly, PCB adducts have blue-shifted absorbance maxima relative to the PΦB adducts. The absorption maximum of recombinant Cph1-PCB in its Pr form is at 656 nm (extinction coefficient ~85,000 M^{-1} cm^{-1} (Lamparter et al., 2001)) and in the Pfr form at 703 nm (both ~12-nm blue-shifted in comparison with Cph1-PΦB (Lamparter et al., 1997)). Cph1 is a histidine kinase involved in two-component signaling (Yeh et al., 1997; Lamparter et al., 2001). Autophosphorylation of the PCB-adduct and transphosphorylation of the response regulator Rcp1 are stronger for the Pr form of Cph1, although in plant phytochromes Pfr is considered to be the physiologically active form (Yeh et al., 1997; Hughes and Lamparter, 1999). Due to its evolutionary relation to plant phytochromes and its advantageous molecular-biological handling properties, Cph1 is a promising system for studies of chromophore assembly, photoconversion, and signal transduction as well as offering an attractive starting point for crystallization for the purpose of x-ray diffraction and structural modeling, serving as a model system for the phytochrome family.

The Cph1-PCB photocycle has been studied by various spectroscopic techniques, including nanosecond time-resolved flash photolysis and steady-state Fourier transform resonance Raman (FT-RR) studies (Remberg et al., 1997), low-temperature fluorescence (Sineshchekov et al., 1998), UV-VIS, and Fourier transform infrared (FTIR) measurements (Foerstendorf et al., 2000) as well as protonation studies (van Thor et al., 2001). Thus, information on the reaction dynamics as well as on structural properties of the chromophore was obtained.

In this paper, the primary photoreaction of Cph1-PCB is investigated by femtosecond time-resolved absorption spectroscopy. These are the first femtosecond studies of a prokaryotic phytochrome. With pulses shorter than 50 fs, the decay of the excited electronic state of the chromophore as well as the decay of the Franck-Condon state, populated by the initial electronic excitation, can be studied in real time. Kinetic models are presented and compared with the corresponding results for plant phytochrome, as described in the literature. The extent to which analogies to the primary reaction dynamics of phytochrome A from plants exist are highlighted.

The photo-induced dynamics of Cph1 reconstituted with PEB (Fig. 1) were also studied. In Cph1-PEB the chromophore $C_{15}{=}C_{16}$ double bond is replaced by a single bond and photoisomerization is inhibited. By comparison of the results for Cph1-PCB with those for Cph1-PCB, effects due to chromophore isomerization alone can be extracted.

MATERIALS AND METHODS

Sample preparation

Phytochrome Cph1 from cyanobacterium *Synechocystis* PCC6803 (open reading frame slr0473) was obtained by expression cloning in *E. coli* (Lamparter et al., 1997). Assembly of the apoprotein with chromophores PCB and PEB was performed as described earlier (Lamparter et al., 1997,

2001; Remberg et al., 1997). The buffer solution used in these experiments was 50 mM Tris, 5 mM EDTA, and 300 mM NaCl at pH 7.8.

The sample concentration was set to <0.4 OD in the spectral maximum of Pr at a path length of 1 mm. The cuvette was sealed with two glass windows (BK7). Because the experiment runs at a repetition rate of 1 kHz, it had to be ensured that predominantly ground-state Pr (Pfr) and no intermediate species were hit by the pump and the probe laser pulses. This was achieved first by rotating the cuvette and moving it up and down perpendicular to the laser beams. Thereby, on average, a given sample volume was excited every 2 s by a laser pulse. Further, appropriate background illumination was applied to assure quantitative photo-induced backreaction; during experiments on the Pr form, background illumination with $\lambda > 715$ nm was applied, and for experiments on Pfr a HeNe laser at 632 nm was used. To check for sample degradation, steady-state absorption spectra were taken before and after the experiments. Additionally, during the experiment, steady-state absorption spectra were taken (in situ, under experimental radiation exposure) at negative delay times between pump and probe pulses; no spectral changes were observed as compared with spectra taken before the experiments. All experiments were performed at room temperature.

Transient absorption

Independently tunable short pump (excitation) and probe pulses were generated by nonlinear optical processes driven by light pulses (160 fs FWHM, 775 nm, 1 kHz repetition rate) from a titanium-sapphire laser system (CPA 2000, CLARK-MXR, Dexter, MI). Excitation of the sample was performed by pulses of a noncollinear optical parametric amplifier (NOPA) (Wilhelm et al., 1997), tunable between 450 and 750 nm. For experiments in the picosecond time regime, probe pulses were provided by a white light continuum, generated by focusing a weak (1–2 μJ) pulse of the laser fundamental at 775 nm into a sapphire plate of 3 mm path length. This set-up allowed a convenient wavelength tuning of the probe light at some expense of time resolution. The typical width of the instrumental response function (IRF: cross-correlation of pump and probe pulse) was 120 fs (FWHM). For experiments in the femtosecond time regime the probe pulses were generated by a second NOPA, resulting in an IRF of typically 45 fs FWHM. For the experiments on Cph1-PCB-Pfr, both excitation and probe pulses were provided by a white light continuum with an IRF of ~500 fs FWHM. The IRF was controlled and measured in all experiments by autocorrelation, cross-correlation, or spectrally resolved Kerr experiments. All experiments except those on the Pfr photoreaction were performed at the magic angle between excitation and probe pulse polarization.

After transmitting the sample, the probe pulses were dispersed in a monochromator and detected by a photodiode. The pump-induced differential absorbance was derived by lock-in amplification of the photodiode signal and chopping the pump beam at half the system repetition rate.

RESULTS

Primary photoreaction of Cph1-PCB-Pr

Cph1-PCB-Pr was excited at 650 nm, i.e., close to the absorption maximum (at 656 nm) and at 615 nm in the high-energy shoulder of the ground-state absorption spectrum. Transient absorbance changes were recorded in the range between 590 and 770 nm up to 500 ps after photoexcitation with high time resolution.

Picosecond time regime

In Fig. 2, kinetic data of Cph1-PCB-Pr are shown as sets of absorbance difference spectra at various delay times between pump and probe laser pulses, with excitation at 650

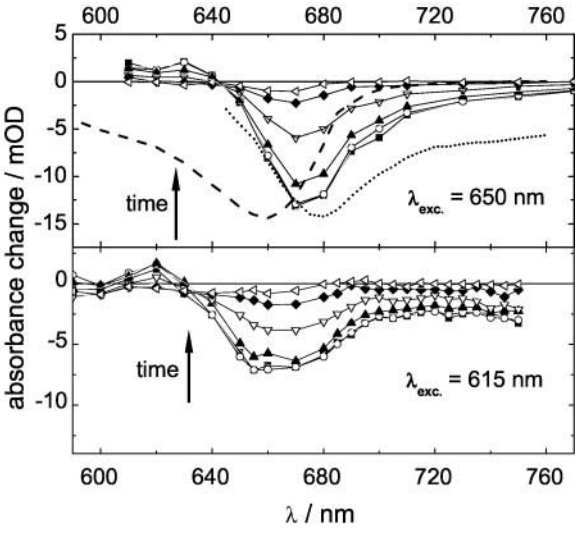

FIGURE 2 Transient absorption-difference spectra of Cph1-PCB-Pr after excitation at 650 nm (*top*) and 615 nm (*bottom*). Spectra are shown at various delay times: 300 fs ■, 1.2 ps ○, 5 ps ▲, 20 ps ▽, 80 ps ♦, and 300 ps ◁. For comparison (*top*) the Cph1-PCB-Pr ground state absorption spectrum (– – –) and the ν^3-corrected fluorescence spectrum (· · ·) are included.

(top) and 615 nm (bottom). To facilitate the interpretation of the spectral features, the inverted stationary ground-state absorption spectrum (GSA, dashed line) and the ν^3-corrected stationary fluorescence (dotted line) spectrum of Cph1-PCB-Pr (Sineshchekov et al., 1998) are displayed as well. At early delay times the difference spectrum exhibits a strong negative band around 670 nm and a weak positive band below 640 nm. The overall signal decays on a time scale of 20–40 ps, without significant change of spectral shape. From visual inspection it is reasonable to regard the transient difference spectra as a superposition of (negative) ground-state bleach, (negative) stimulated emission (SE), and (positive) excited electronic state absorption (ESA). Especially, SE contributes significantly to the long wavelength part of the difference spectra, whereas ESA cancels partly the short wavelength part of the ground-state bleach and dominates below 640 nm. Other contributing intermediate states, e.g., a reaction product in the electronic ground state, cannot be identified readily. However, it should be noted that with excitation at 615 nm the transient negative band in Fig. 2 is slightly broader than with excitation at 650 nm. After 300 ps, the difference signal has decayed almost to zero, showing positive sign around 700 nm and negative sign around 665 nm. Taking into account a forward reaction quantum yield of 15% for Cph1-PCB-Pr (Lamparter et al., 1997), this indicates already that the spectrum of the first electronic ground-state photoproduct of Cph1-PCB-Pr shows strong overlap with the Pr electronic GSA.

Initially, kinetic analysis of the transient difference absorption curves was carried out at individual probe wave-

TABLE 1 Summary of the fit parameters obtained from the analysis of the Cph1-PCB-Pr reaction dynamics on the picosecond time scale with excitation at 650 and 615 nm, respectively

λ_{exc}/nm	Fit function	Best values	95% probability of match
650	(I) $N = 2$	$\tau_1 = 11.7$ ps; $\tau_2 = 48$ ps	$\tau_1 = 8.0$–14.8 ps; $\tau_2 = 32$–88 ps
	(II)	$\tau = 15.7$ ps; $n = 1.9$	$\tau = 14.5$–17.1 ps; $n = 1.5$–2.7
615	(I) $N = 2$	$\tau_1 = 15.1$ ps; $\tau_2 = 97$ ps	$\tau_1 = 5.1$–22.0 ps; $\tau_2 = 35$–300 ps
	(II)	τ=19.6 ps; $n = 1.32$	$\tau = 15.4$–23.5 ps; $n = 0.8$–2.0

Listed are the time constants τ_i based on a sum of two exponentials (model I) and the time constants τ for the chosen distribution of rate constants (model II). The time constants of model I can be regarded as a measure of the width of the respective distribution (model II). The second moment of the distribution (model II) is proportional to $1/\sqrt{n}$. The last column gives the range of 95% probability for match with the true value.

lengths. Then, the data were analyzed globally. For the latter, two fit models were employed and tested. Model I (Eq. 1) describes the observed absorption difference $\Delta A(t, \lambda)$ by a sum of $N = 2$ exponentials:

$$\Delta A(t, \lambda) = A_0(\lambda) + \sum_1^N A_i(\lambda) \times e^{-t/\tau_i}, \qquad (1)$$

with apparent time constants τ_i and amplitudes A_i. The wavelength-dependent quantities $A_i(\lambda)$ are the decay-associated spectra (DAS) used below. Model II (Eq. 2) assumes the following distribution $f(k)$ of rate constants:

$$f(k) = \frac{(n\tau)^n k^{n-1}}{\Gamma(n)} e^{-n\tau k}, \qquad (2)$$

where k_0 is its first moment ($\tau = 1/k_0$) and n determines its width ($k_0/\sqrt{n}$) is proportional to its second moment). The Laplace transform of $f(k)$:

$$\Delta A(t, \lambda) = A_0(\lambda) + A_1(\lambda)\left(1 + \frac{t}{n\tau}\right)^{-n}$$

was used as fit function. The specific distribution of rate constants $f(k)$ used (Eq. 2) was chosen for practical mathematical reasons. It has an asymmetry with respect to its maximum and serves as a first approximation to the true distribution. In a reverse procedure the true distribution of rate constants could be obtained by an inverse Laplace transform of the absorption transients. Unfortunately, an inverse Laplace transform is numerically ill conditioned, and additional numerical procedures (McWhirter and Pike, 1978) have to be applied to get a reasonable set of rate constants.

In a first analysis using model I, the monoexponential ($N = 1$) and the triexponential ($N = 3$) case could be rejected. For $N = 1$, large residuals resulted between fit and the experimental data, which could be eliminated with the $N = 2$ fit. For $N = 3$, unambiguousness of the resulting fit parameters could not be established. An exhaustive search analysis (χ^2) revealed that model I and model II describe the experimental data equally well. The parameters of the best fits for each model are summarized in Table 1. In Figs. 3 and 4 the fit results according to model I with $N = 2$ and model II are given. Depicted are the respective DAS $A_i(\lambda)$ for excitation at 650 nm (Fig. 3) and 615 nm (Fig. 4) together with the fit parameters as an inset. The constant DAS $A_0(\lambda)$ represent the difference spectra at long delay times, i.e., the difference between the photoproduct and the initial Pr GSA. $A_1(\lambda)$ and $A_2(\lambda)$ represent the reaction dynamics. The two DAS $A_1(\lambda^{650})$ and $A_2(\lambda^{650})$ in the biexponential model for excitation at 650 nm do not show significant spectral differences. With excitation at 615 nm, differences in the relative amplitudes of $A_1(\lambda^{615})$ and $A_2(\lambda^{615})$ are observed. However, their overall trend and sign are the same and the χ^2 analysis indicates (not shown) that $A_1(\lambda^{615})$ and $A_2(\lambda^{615})$ become alike in shape when varying the respective time constants within the confidence interval of 95%. On these grounds, our results show that in the picosecond time regime the decay of the excited electronic state and of the stimulated emission, the Pr ground-state recovery and product formation exhibit all the same kinetics. In other words, the respective kinetic components of model I and model II are associated with molecular species of almost identical spectral characteristics concerning the respective contributions from SE and ESA. This indicates that both kinetic components (of model I) belong to loca-

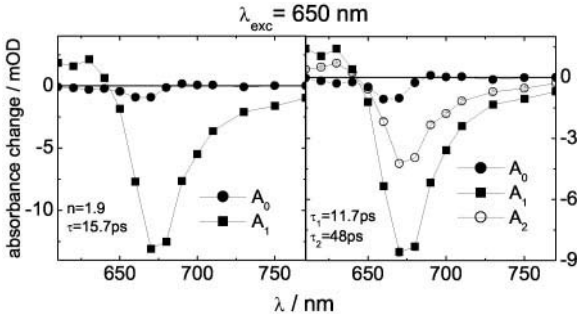

FIGURE 3 DAS A_i of the Cph1-PCB-Pr reaction dynamics (excitation at 650 nm) as evaluated from two fit models. (*Left*) Distribution of rate constants (model II); (*Right*) Sum of two exponentials (model I). The fit parameters are also listed in Table 1. See Results for definition of DAS. The height of the symbols represents the statistical error of the DAS at fixed decay times τ_i.

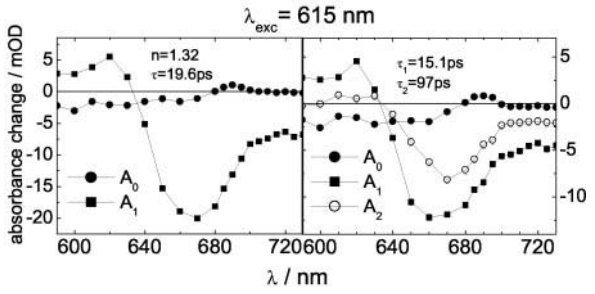

FIGURE 4 DAS A_i of the Cph1-PCB-Pr reaction dynamics as in Fig. 3 but with excitation at 615 nm.

tions on very similar excited-state potential energy surfaces. By this count a heterogeneous excited-state distribution seems likely. This observation favors the use of a distribution of rate constants as in model II. In addition, model II achieves the same χ^2 by a reduced (by 1) number of fit parameters as compared with the biexponential model I. Furthermore, a distribution of rate constants is highly plausible for a chemical reaction under conformational constraints as they occur in proteins. Similar models have been applied successfully to ligand binding in heme proteins (Austin et al., 1975; Fraunfelder and Wolynes, 1985). The underlying concept is that of a distribution of conformational protein substates and a correspondingly shaped potential energy surface (landscape). Here we suggest that for a given excitation energy the postulated distribution of conformational states is associated with a distribution of kinetic components with very similar spectral characteristics. Excitation at shorter wavelength transfers more energy to the excited electronic state and is supposed to lead to slightly changed kinetics and transient spectra (see below).

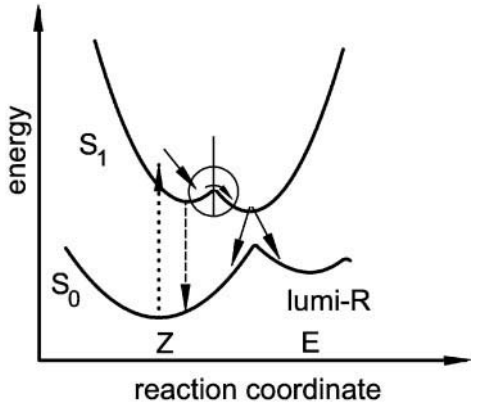

FIGURE 5 Simplified energy level diagram of the photo-induced reaction of Cph1-PCB-Pr. Included are photoexcitation (· · ·), fluorescence (– – –), fast relaxation and a barrier on the S_1 surface, and finally the branching reaction toward the product state lumi-R and the Pr ground state. The circle at the barrier symbolizes a distribution of barrier heights leading to a distribution of barrier-crossing rate constants.

In summary, the following scenario (see also energy level scheme in Fig. 5) is suggested for the primary photoreaction of Cph1-PCB-Pr. Following fast relaxation processes in the excited electronic state within 100–200 fs (see below) a local minimum on the S1 surface is reached. From here a barrier has to be overcome to achieve isomerization and transition to the Pr electronic ground state and the product electronic ground state, respectively, according to a reaction quantum yield of 15% (Lamparter et al., 1997). The barrier can be overcome by thermal energy and favors again a distribution of rate constants. With model II the first moment of this distribution amounts to $(15.7\ \text{ps})^{-1}$ (excitation at 650 nm), but corresponding to its width of $n = 1.9$, significant components of k are found in a much broader range, i.e., that found in the biexponential fit (model I) between $(8\ \text{ps})^{-1}$ and $(88\ \text{ps})^{-1}$ (cf. Table 1). The existence of an activation barrier in the S_1 state was proposed earlier from temperature-dependent and static fluorescence spectroscopy (Sineshchekov et al., 1998) of Cph1-PCB-Pr with an activation energy of 5.4 kJ/mol and from resonance Raman studies of oat phytochrome (Andel et al., 1996).

The distribution of reaction rates can be caused by a heterogeneous distribution of Pr ground-state molecules in different conformational substates (see below). On the other hand, a distribution can also be created in the excited electronic state in response of the chromophore binding pocket to the electronic excitation, e.g., by breakage of hydrogen bonds and reorganization of amino acid residues or protein-bound water molecules.

Excitation at 615 nm instead of 650 nm leads to a slightly broadened ($n = 1.32$ instead of 1.9) distribution $f(k)$ and a slightly decreased first moment ($(19.6\ \text{ps})^{-1}$ instead of $(15.7\ \text{ps})^{-1}$); i.e., smaller as well as larger time constants are observed, but on average the reaction slows down (cf. Table 1). The broadening of the distribution of rate constants can be explained by dynamic effects. With shorter excitation wavelength, more energy is fed into the excited state, which may result in an altered, e.g., broader variety of protein responses, and thus in a broader distribution of conformational states with different potential energies. This picture is consistent with 1) the observation (cf. Figs. 3 and 4) that the DAS $A_1(\lambda^{615})$ is broader than $A_1(\lambda^{650})$, 2) the widths of the respective calculated excited ESA (Fig. 6, see below), and 3) the observation (Roelofs, Robert-Rössle-Klinik, Berlin, personal communication) that the steady-state fluorescence of Cph1-PCB-Pr broadens by ~5 nm when exciting at 630 nm instead of 670 nm. Within this picture an excitation-energy-dependent reaction quantum yield might be expected, but to our knowledge this has not been observed. The broadening of the distribution $f(k)$ at higher excitation energy might also reflect a distribution of Pr ground-state conformations. This would show up in Pr-Pfr difference spectra when the Pr→Pfr transition is carried out at different excitation wavelengths, whereby different

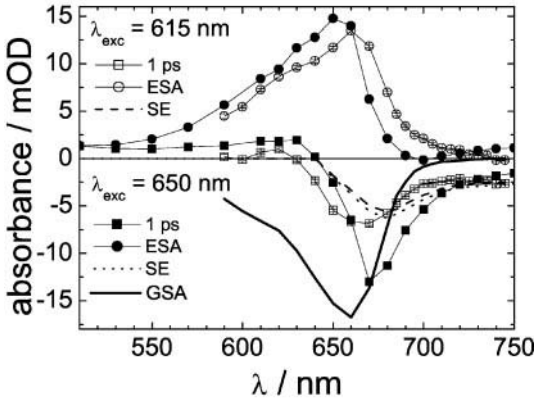

FIGURE 6 Calculated spectra of the ESA after excitation of Cph1-PCB-Pr at 650 nm (●) and 615 nm (○). The spectra represent a weighted sum of the respective Pr difference spectrum after 1 ps, the GSA, and the SE spectrum (ν^3-corrected fluorescence).

sub-ensembles of the Pr state would be transformed to respective sub-ensembles of the Pfr state. To our knowledge, such a wavelength-dependent effect has not been observed either. Thus, either the Pr ground-state heterogeneity is small or fast equilibration occurs on the time scale of the Pr→Pfr transition. However, indications of a limited heterogeneity are given in the DAS $A_0(\lambda^{650})$ and $A_0(\lambda^{615})$ in Figs. 3 and 4 as well as in the late difference spectra of Fig. 7. $A_0(\lambda^{615})$ exhibits stronger negative contributions on the high-energy side than $A_0(\lambda^{650})$. On the other hand, the zero crossing of the signal in the difference spectra (Fig. 7) at 680 nm is the same for both excitation wavelengths. In any case, the respective signals are small and the differences can hardly be regarded as significant. Therefore, the heterogeneity of the Pr ground state results at most in a narrow distribution.

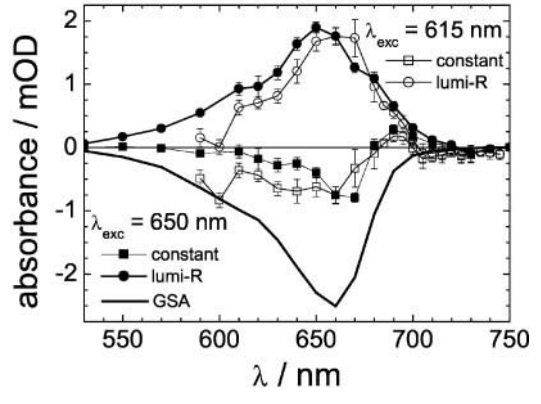

FIGURE 7 Calculated spectra of the photoproduct (lumi-R) after excitation of Cph1-PCB-Pr at 650 nm (●) and 615 nm (○). The spectra represent a weighted sum of the respective Pr GSA and the late difference spectrum (constant) as described in the text.

Excited electronic state and photoproduct

The absorption spectra of the excited electronic state and of the ground-state photoproduct can be obtained approximately from the transient difference spectra (Fig. 2), the Pr electronic GSA, and the ν^3-corrected stationary fluorescence spectrum of Cph1-PCB-Pr (Sineshchekov et al., 1998). At long delay times the experimental difference spectrum is a superposition of only the Pr GSA and the ground-state spectrum of the photoproduct. To obtain a fairly smooth and only single-peaked and positive spectrum, a certain fraction of the Pr GSA (κGSA) was added to the temporally constant difference absorption spectrum. This procedure is arbitrary to some extent but seems appropriate to give a rough idea about the spectrum of the photoproduct (Fig. 7). As already indicated by the small amplitude of the late difference absorption spectra, the resulting product spectra (obtained for excitation at 650 and at 615 nm) reproduce closely the shape of the Pr absorption spectrum (GSA) as included in Fig. 7 for comparison. On the time scale of our experiments (500 ps) no further changes in the signal amplitude were observed. Hence, the photoproduct is identified with a form of lumi-R as it has been characterized for plant phytochromes by time-resolved and low-temperature absorption studies (Braslavsky et al., 1980; Eilfeld and Rüdiger, 1985; Cordonnier et al., 1981; Ruzsicska et al., 1985; Inoue et al., 1990; Scurlock et al., 1993a,b; Zeidler et al., 1998).

Similarly, the spectrum of the excited electronic state can be calculated from the early experimental difference spectrum. The latter consists of contributions from Pr ground-state bleach, SE, and ESA. Knowing the residual amount of Pr GSA at late times (κGSA) and the Cph1-PCB-Pr reaction quantum yield of 15%, the initial amount of Pr GSA in the early difference spectra was determined and subtracted from the difference spectra averaged in the 0.5–1.9-ps time window. Next, the contribution of stimulated emission was subtracted by adding a suitable amount of the ν^3-corrected stationary fluorescence spectrum of Cph1-PCB-Pr until an entirely positive spectrum was obtained. Again, this procedure is arbitrary to some extent because the amount of SE cannot be determined accurately. The approximate ESA spectra (650- and 615-nm excitation, respectively) are shown in Fig. 6. They peak at ~660 nm with a small red shift (<10 nm) and a small broadening (~6 nm) when exciting at 615 nm.

In comparison, the spectrum of the product (Fig. 7) and the excited state (Fig. 6) show considerable overlap with the Pr ground-state spectrum. With respect to the latter, the product spectrum extends more to the red as indicated already in the late difference spectra in Fig. 2. The excited-electronic-state spectrum, however, extends to the blue and to the red part of the spectrum up to 900 nm (data not shown). It cannot be excluded, though, that excited state and product state carry oscillator strength in parts of the spec-

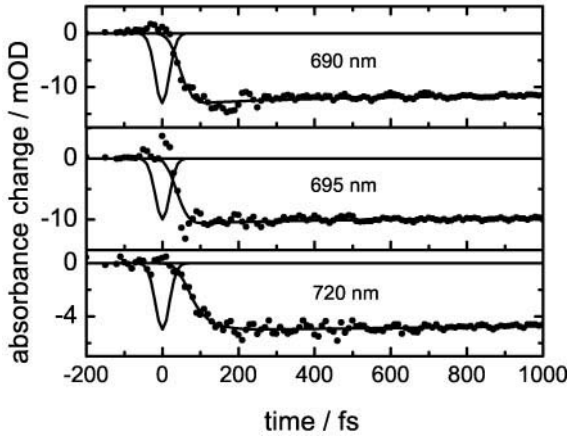

FIGURE 8 Absorption transients of Cph1-PCB-Pr after excitation at 650 nm at three probe wavelengths as indicated. Shown are the experimental data, the instrumental response function, and fits involving a sum of exponentials, convoluted with the instrumental response function.

trum not examined here, i.e., outside the range of 430–900 nm.

Femtosecond time regime

The experiments on the time scale below ~1 ps were performed using a NOPA for excitation and another one for probing, resulting in a shorter instrumental response function of ~45 fs FWHM. In Figs. 8 and 9, absorption transients of Cph1-PCB-Pr at different probe wavelengths after excitation at 650 and 615 nm, respectively, are shown together with the instrumental response function. The probe laser covers the range from 670 to 720 nm. The negative sign of the signals indicates that they are dominated by ground-state bleach and/or SE. With increasing wavelength, the relative amount of SE increases with respect to the contribution of ground-state bleach (cf. Figs. 2 and 6). The main feature of all kinetics shown is a delayed rise of the signals. The data were fitted with a sum of exponentials convoluted with the IRF. The kinetics appear to be composed of a delayed onset of the signal and at least one exponential term in the fit function, characterized by a small amplitude and a time constant of ~150 ± 100 fs at both excitation wavelengths. At 300 fs after experimental time 0, a signal level is reached that is stationary on the time scale of a few picoseconds. The decay is characterized by the longer time constants described above.

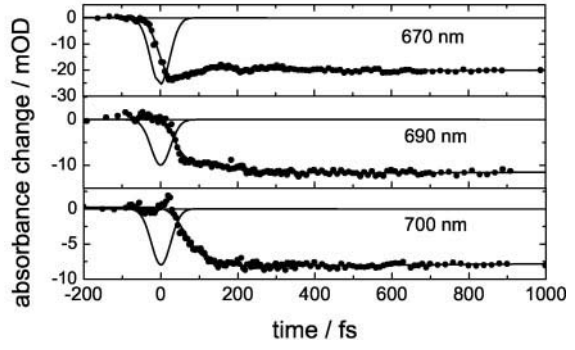

FIGURE 9 Absorption transients of Cph1-PCB-Pr after excitation at 615 nm at three probe wavelengths as indicated. Shown are the experimental data and fits involving a sum of exponentials, convoluted with the instrumental response function.

In general, photoexcitation of a protein-bound chromophore is followed by fast intra- and intermolecular relaxation processes that transform the system from the initially populated Franck-Condon states to the respective equilibrium structure. If the excitation is fast enough, the response of the molecular system will consist of a coherent part and a dissipative part. Coherent nuclear motion along specific vibrational modes occurs with the propagation of the wave packet that is initially formed by the short and hence spectrally broad excitation laser pulse. Indication for such a wave-packet motion is given by oscillatory components in the transient absorption signal as shown in Fig. 8. They fade away within the first picosecond, are of small amplitude, and do not show a regular periodic pattern; i.e., they consist in a superposition of contributions with different oscillatory periods. Here it should only be noted that despite the large number of vibrational degrees of freedom as found in a system like the tetrapyrrole in the Cph1 protein, a coherent component is still discernible. Similar observations have been reported for other chromoproteins such as photosynthetic reaction centers (Spörlein et al., 1998; Vos et al., 2000) and retinal proteins (Ye et al., 1999; Wang et al., 1994; Zinth et al., 2000). Excited-state and ground-state dynamics seem to be sufficient for their interpretation.

The dissipative component of the molecular response comprises processes such as energy relaxation into the vibrational manifold and orientational relaxation of the surrounding amino acid residues and water molecules leading to a fluorescence Stokes shift of ~20 nm in Cph1-PCB-Pr. Our results demonstrate fast relaxation processes of this type in Cph1-PCB-Pr on a time scale of a few hundred femtoseconds. Kinetically, they are clearly separated from the slower processes on the picosecond time scale.

Primary photoreaction of Cph1-PCB-Pfr

The reaction cycle of Cph1-PCB is completed by a second photoreaction that converts the stable product Cph1-PCB-Pfr back to Cph1-PCB-Pr via several thermally driven reaction steps. The quantum yield of this phototransformation has been determined to 15% (Lamparter et al., 1997). We carried out transient absorption experiments with excitation at 727 nm and selected probe wavelengths at 690, 710, and 760 nm. Because the sample is driven into a Cph1-PCB-Pr/Pfr mixture during the experiment, care had to be taken to

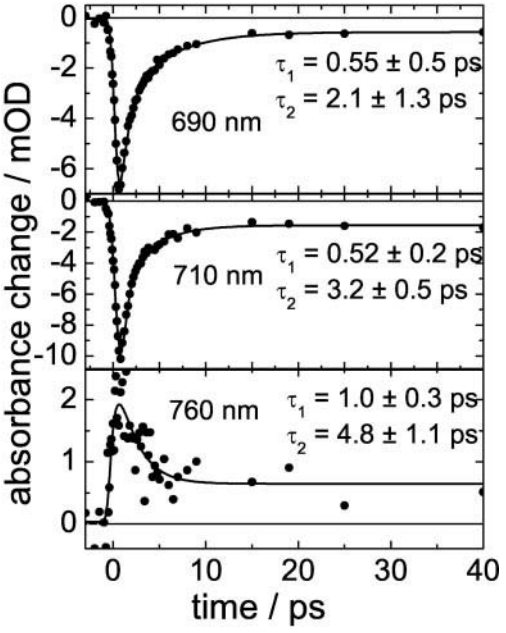

FIGURE 10 Absorption transients of Cph1-PCB-Pfr after excitation at 727 nm at various probe wavelengths. Shown are the experimental data and fits by a sum of two exponentials, convoluted with the instrumental response function. Note that at 690 and 710 nm, τ_1 and τ_2 are decay times whereas at 760 nm, τ_1 is a rise time and τ_2 is a decay time. The global fit yields time constants of 0.54 and 3.2 ps.

minimize the amount of Cph1-PCB-Pr and selectively to excite the Pfr form. This was achieved by background illumination at 632 nm, where depletion of Pr is more efficient than for Pfr, and by long-wavelength pump at 727 nm, where Pr does not absorb. In this case the absorption transients are well fitted by a sum of exponentials (model I), convoluted with the IRF of ~500 fs FWHM. The experimental data and the fit results are shown in Fig. 10. The instantaneous rise of the negative signals at 690 and 710 nm is followed by a biexponential decay with time constants around 0.5 ps and 2–5 ps. At 760 nm, the positive signal rises with a time constant of ~1 ps and decays with ~5 ps. A global fit renders the two time constants 540 ± 20 fs and 3.2 ± 0.4 ps. The residual signal amplitudes at long delay times are stationary on the time scale of our experiment, i.e., 40 ps. The observed positive and negative signals represent the contributions of ground-state bleach and SE (to the negative) and the contribution of ESA and photoproduct absorption (to the positive). Our results show the existence of two consecutive reaction steps that follow photoexcitation and lead to the first electronic ground-state product. In comparison with the Pr photoreaction, the Pfr photoreaction is significantly faster. The picosecond dynamics is biphasic and cannot be fitted with a single distribution of rate constants as the picosecond dynamics of the Pr photoreaction because formation and decay of an intermediate state are observed (at 760 nm, Fig. 10, bottom). This does not exclude the existence of a distribution of rate constants for each of the observed reaction steps. Due to the lower time resolution of this experiment, faster (<500 fs) relaxation steps depopulating the Franck-Condon states cannot be resolved but might nevertheless exist. Furthermore, the question as to whether both observed steps occur on the excited-state surface or partly on an electronic ground-state surface cannot be answered from these results.

Cph1-PEB as a probe for chromophore protein interaction

PCB and PΦB are natural bilin chromophores of Cph1 and plant phytochrome. PEB assembles also with apo-phytochromes (Li et al., 1995) but may be regarded as a blocked chromophore with the $C_{15}{=}C_{16}$ double bond replaced by a single bond. PEB adducts are thus unable to undergo the initial photoisomerization step of PCB and PΦB adducts, a side effect being the high fluorescence quantum yield of PEB adducts with a lifetime of ~2 ns (Murphy and Lagarias, 1997). Because PEB binds in the same protein environment as PCB, Cph1-PEB can be used to study chromophore-protein assembly processes as well as non-isomerizing dynamics induced by photoexcitation. Because no Z-E isomerization takes place, the processes due to isomerization can be separated and insight into the different effects of chromophore-protein interaction can be obtained.

Transient absorption experiments with Cph1-PEB were performed with excitation in the GSA maximum at 580 nm and probe wavelengths between 455 and 710 nm with an IRF of 80 fs FWHM. The fit of the absorption transients on the time scale of up to 400 ps with an instant rise and single-exponential decay render a time constant between 0.7 and 2.0 ns (data not shown). This is in accordance with fluorescence lifetime measurements on several PEB-binding phytochromes (Murphy and Lagarias, 1997). Difference spectra on the (slow) picosecond time scale are shown in Fig. 11. The experimental difference spectrum taken at 60 ps after excitation is shown together with a simulation by a weighted sum of GSA (bleach) and ν^3-corrected fluorescence (stimulated emission). The shoulder in the experimental difference spectrum at 540 nm is taken to determine the contribution of GSA, the peak at around 570 nm and the low-energy side then determine the contribution of SE. The simulation yields the spectrum of the excited electronic state, which peaks at ~470 nm.

In a second set of experiments the femtosecond time scale was investigated. In Fig. 12, an absorption transient taken at 640 nm is shown as an example. At this wavelength, the SE dominates the observed signal. To guide the eye, the experimental data are shown together with a simulation, using a delayed (40-fs) but instant rise of the signal, convoluted with the IRF. The small Stokes shift of ~8 nm (cf. Fig. 11) might explain that in our experiments it was not possible to clearly distinguish between a rise time of the signal (40–150

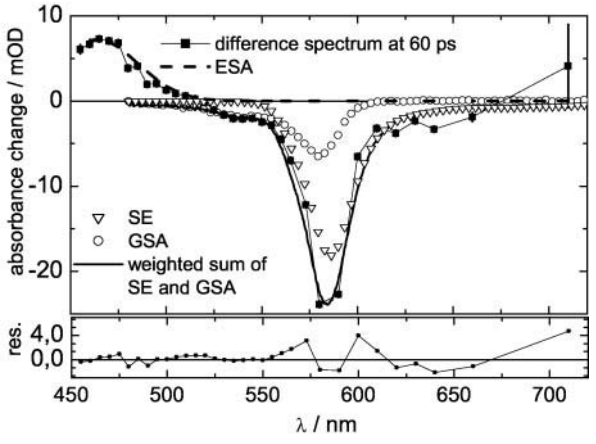

FIGURE 11 Experimental difference absorption spectrum of Cph1-PEB, 60 ps after excitation at 580 nm (■). Simulation (——) of the negative part of the spectrum is achieved by adding contributions of the GSA (○) and SE (ν^3-corrected fluorescence, ▽). The positive part due to the excited ESA was fitted with a Gaussian line shape (— — —) with peak at 467 nm. The residuum (*bottom*) shows the difference between the experimental data and the sum of GSA, SE, and ESA.

ps) and a delayed onset. Besides this observation, the data on Cph1-PEB give no indication of further fast processes on the time scale longer than 150 fs, as in Cph1-PCB.

DISCUSSION

For the study of mechanisms that govern the control of photoreactions by the protein, phytochrome is an attractive system because both the Pr→Pfr and the Pfr→Pr photoreaction occur in the same protein binding pocket. In principle, this provides the special opportunity to characterize the control mechanisms for two reaction pathways in one protein environment as compared with the usual one-way protein-based photoreactions. In the current lack of structural information about phytochrome at atomic resolution, the interpretation of spectroscopic data concerning structure-function relationships is limited. Nevertheless, comparison of the primary reaction dynamics involving different chromophore configurations, chromophore structures, and protein environments provide insight into chromophore-protein interaction and catalytic influence of the chromophore binding pocket.

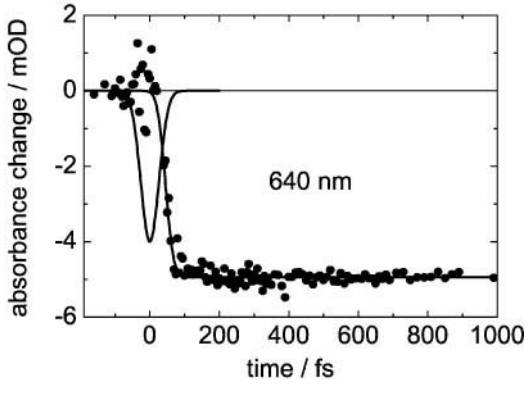

FIGURE 12 Femtosecond absorption transient of Cph1-PEB probed at 640 nm after photoexcitation at 580 nm. The data are simulated with a delayed (40 fs) but instantaneous rise and a decay on the nanosecond time scale, including the convolution with the instrumental response function of 80 fs FWHM.

The major result of this work is the characterization of the photo-induced fast reaction dynamics of Cph1-PCB in the Pr and the Pfr states. After fast (~150-fs) relaxation processes in the excited electronic state Pr*, the reaction is preferably described by a distribution of rate constants centered at $(16\ \text{ps})^{-1}$ that leads to the product (and educt) electronic ground state after crossing a barrier. The Pfr photoreaction is faster and best characterized as biexponential with two time constants of 0.54 and 3.2 ps. Because the experiments described in this work are the first of this kind on a bacterial phytochrome, it is important to compare the results with the appreciable wealth of data accumulated for plant phytochrome A as described in the literature. Moreover, the femtosecond data extend the studies of the Cph1-PCB reaction cycle reported so far into the picosecond and femtosecond time regime. Both aspects are discussed in the following.

Comparison with plant phytochrome A

The fast, primary photoreactions of plant PhyA-Pr have been studied extensively, although described controversially in the literature. Picosecond time-resolved pump-probe experiments on pea phytochrome A (Kandori et al., 1992) revealed a single time constant of 24 ps for product formation and excited-state decay, whereas similar experiments on oat phytochrome A (Savikhin et al., 1993) resulted in a biphasic dynamics with time constants of 16 and 50–60 ps. In Andel et al. (1997), it was concluded from transient absorption experiments that the description of the picosecond reaction dynamics of oat-phytochome-PΦB-Pr requires only a single time constant of 24 ps. Nevertheless, a biexponential fit of these transient absorption data is possible and reveals time constants of 13 and 44 ps. However, the second component was attributed to the dynamics of a molecular species formed during the experiment by photodegradation of the sample as observed by monitoring the absorption spectrum of Pr. First, the observed time constants fit qualitatively those observed in our experiments, i.e., 21 ps for a monoexponential fit (data not shown) and 12 and 48 ps, respectively, for a biexponential fit (cf. Table 1). Second, in our experiments, photodegradation was not observed and a biexponential fit in the picosecond time regime clearly gives a better result than a monoexponential fit. Considering that in the experiments of Andel et al. (1997) the average time between re-excitation of a specific sample volume was possibly as short as 0.2 s (in our experiments,

2 s), full recovery of the photocycle may have been a problem. Intermediate states could have influenced the dynamics measured. Thus, the results of Andel et al. (1997) are neither consistent nor inconsistent with our results.

Transient absorption data on PΦB-PhyA-Pr from oat by Hermann and co-workers (Rentsch et al., 1997; Bischoff, 2000; Bischoff et al., 2001) are described by two kinetic components in the picosecons time regime. The DAS (2–3 ps and ~30 ps, respectively) are shifted by ~10 nm with respect to each other. In addition, a sub-picosecond time constant of 150–360 fs was determined and a delayed rise of SE as well as of ESA was observed on the low-energy side and the high-energy side of the Pr GSA, respectively (Büchler et al., 1995). From time-resolved fluorescence experiments also, biphasic kinetics were reported with time constants of 14 and 45 ps (Hermann et al., 1990). A sequential reaction scheme was proposed involving a fast relaxation on the S_1 surface, two successive reaction steps (2 and 30 ps), and finally the branching reaction to the product and Pr ground state. Again, the time constants in the range between 10 and 40 ps correspond to our results. On the other hand, time constants as short as 2–3 ps fall outside the 95% probability range in the analysis of our data. This discrepancy might originate in the structural differences between oat phytochrome A and Cph1-PCB or in additional reorientational dynamics corresponding to the fast 3-ps component.

Further ultrafast transient absorption experiments (Müller and Holzwarth, (see above) personal communication) as well as time-resolved fluorescence experiments (Holzwarth et al., 1984, 1992) have been performed on PΦB-PhyA-Pr from oat. From the fluorescence measurements, excitation-wavelength-dependent sets of decay time constants were determined: 5 ps, 45 ps, and 194 ps at 640-nm excitation and 11 ps, 44 ps, and 160 ps at 660-nm excitation. The fluorescence maxima were found between 680 and 690 nm. For the analysis of the transient absorption data, the approach of a Laplace transform of the entire data set was chosen. The result is a distribution of rate constants with significant contributions between $(15\ \text{ps})^{-1}$ and $(50\ \text{ps})^{-1}$. On the femtosecond time scale, kinetics with time constants of ~100 fs were observed. Both the time constants from fluorescence and from transient absorption data agree qualitatively with our results. The changes of the time constants deduced from the fluorescence decay are consistent with our observation of a broadening of the distribution $f(k)$ when exciting at shorter wavelength. The stated width of the distribution of rate constants in recombinant oat-PhyA-Pr with PΦB- and PCB-chromophores, respectively, was in accordance with our findings on Cph1-PCB-Pr. Equally, the sub-picosecond time constants found in oat-phytochrome-Pr are consistent with those found in Cph1-PCB-Pr, although in the latter, the strong spectral overlap between ESA and stimulated emission prevented the disentanglement of the contributing processes.

Our results on the Pfr photoreaction are in qualitative accordance with results for oat-PΦB-PhyA-Pfr in the literature (Müller and Holzwarth, (see above) personal communication; Bischoff et al., 1998, 2001; Rentsch et al., 1998; Bischoff, 2000). The Pfr photoreaction is reported to follow a sequential dynamics described by time constants in the range between 150–650 fs and 2–5 ps.

A general difference between plant phytochrome A and Cph1-PCB concerns not only the absolute but also the relative positions of the maxima of the Pr-, lumi-R, and Pfr absorption bands. In type A plant phytochromes and in Cph1, the absorption spectra of the Pr and Pfr forms undergo a blue-shift of ~10–14 nm when exchanging PΦB by PCB (Schmidt et al., 1996; Remberg et al., 1997). Beyond it, the spectra of Cph1-PCB-Pfr and the first photoproduct of the Pr form (lumi-R, see below) exhibit an additional 10–30-nm blue-shift as compared with the respective spectra in oat PhyA phytochrome (in oat-phytochrome-PΦB the λ_{max} values of Pr, lumi-R, and Pfr are 665, 680, and 730 nm, respectively (Bischoff, 2000), whereas in Cph1-PCB the respective λ_{max} values are 656, ~660, and 703 nm (see above)). In other words, the λ_{max} of lumi-R and Pfr in Cph1, presumably both in C_{15}-E configuration (see below), are closer to the λ_{max} of the parent-state Pr than the λ_{max} of the lumi-R and Pfr in oat-PhyA. This difference is likely to reflect distinct structures of the chromophore binding pocket in PhyA and Cph1, which apparently affect the static, spectral properties of the C_{15}-E configurations more than the respective kinetics. Possibly, the same structural motif is responsible for the increased blue-shift of the Cph1-PCB-Pfr spectrum and that of the first photoproduct.

In summary, the fast dynamics reported for plant phytochrome A agree qualitatively with our observations on Cph1-PCB. This concerns both, the Pr→Pfr and the Pfr→Pr photoreaction at room temperature with the exception that a time constant of 2–3 ps seems to be absent in the Cph1-PCB-Pr data. Especially the persistent observation of at least two time constants between ~10 and 50 ps is consistent with the picture of the Cph1-PCB-Pr reaction dynamics obtained in this work, i.e., either a relatively broad distribution of rate constants or multiexpoential sequential reaction kinetics. It appears as characteristic for both plant phytochromes and Cph1-PCB that at room temperature the ultrafast photo-induced isomerization dynamics show a relatively slow Pr photoreaction (possibly better described by a distribution of rate constants), whereas the pronounced biexponential Pfr photoreaction is relatively fast. This similarity in the fast photodynamics of plant phytochrome and Cph1 may be of interest from an evolutionary point of view. Of known prokaryotic phytochrome-like proteins, Cph1 is the closest relative to plant phytochromes, yet it is much more distant from the plant phytochrome group than is any plant phytochrome. Thus, it is remarkable that at room temperature the basic properties of the photo-in-

duced reaction dynamics of plant and cyanobacterial phytochromes are very similar.

Chromophore-protein interaction and isomerization

The effect of the protein environment on the reaction dynamics of the chromophore is demonstrated by comparison of the protein-bound photoreaction and the photoreaction in solution. Experiments on the photo-induced reaction dynamics of PCB in solution (Bischoff et al., 2000) show time constants of 3 and ~30 ps, which are attributed to different chromophore configurations. These observations are in contrast to our findings regarding the dynamics of the Pr as well as the Pfr photoreaction and point at the specification of the photoreaction by the protein environment. Because no structure of phytochrome at atomic resolution is available, the direct comparison of chromophore structures and related time constants is not possible. However, information about the chromophore-protein interaction can be obtained from the experiments on Cph1-PEB, in which isomerization is inhibited. In PEB, the conjugated π-electron system is truncated between rings C and D in comparison with PCB; thus, ring D is electronically decoupled. This leads to a blue-shifted GSA but might as well be the reason for the smaller fluorescence Stokes shift of ~8 nm as compared with ~20 nm in Cph1-PCB-Pr (cf. Figs. 2. and 11). Further, in Cph1-PEB the ESA appears centered at 466 nm, ~100 nm blue-shifted with respect to the GSA, whereas in Cph1-PCB-Pr both spectra show considerable spectral overlap. This could indicate that the interaction between the chromophore and its protein binding pocket in Cph1-PCB-Pr is of a more rigid nature along rings A–C and of a more flexible nature around ring D where isomerization takes place.

In contrast to Cph1-PEB, isomerization takes place in Cph1-PCB, and the experiments described here observe the excited state and its decay into the product states for the photoreactions of both the Pr and the Pfr form of cyanobacterial phytochrome (Cph1-PCB). The product states are precursors of or even identical with the lumi-R (Remberg, 1997) and lumi-F (Foerstendorf et al., 2000) intermediates, respectively, suggested as early intermediate states in the course of the Pr and Pfr photoreaction of Cph1. Lumi-F was characterized by low-temperature trapping experiments (Foerstendorf et al., 2000). Lumi-R cannot be trapped in this way (Sineshchekov et al., 1998; Foerstendorf et al., 2000), and at low temperatures its photochemical activity is inhibited in Cph1-PCB-Pr, whereas in oat phytochrome it persists (Sineshchekov et al., 1998). This was attributed to a heterogeneity of the Pr ground state of oat phytochrome (Sineshchekov, 1995a,b). According to this model, two types of PhyA exist, phyA′ and phyA″, with different activation barriers E_a in the excited electronic state, i.e., some hundred J/mol and 4.5 kJ/mol, respectively. Cph1-PCB resembles type A″ and phyB, which shows reduced reactivity at lower temperatures. It is assumed that the high activation barrier in Cph1-PCB is linked to the Z-E isomerization and is caused, e.g., by steric constraints in the protein binding pocket or stronger hydrogen bonding between chromophore and protein. This picture (Sineshchekov et al., 1998) is consistent with our observations.

The question is when the C_{15} double bond isomerization takes place in the course of the Cph1-PCB-Pr and -Pfr photoreaction. This cannot be answered directly by the experiments described here. But the close similarities between RR and FTIR spectra of oat-phytochrome-Pr and Cph1-PCB-Pr as well as between those of the respective Pfr states (Matysik et al., 1995; Foerstendorf et al., 1996, 2000; Remberg et al., 1997) indicate that rotation of ring D, established for the lumi-R state of oat phytochrome, is also accomplished in the lumi-R state of Cph1-PCB. However, torsional dynamics of the chromophore in plant phytochrome in general and in particular the state of rotation or isomerization around the C_{15} single bond connecting rings C and D is currently under discussion (Matysik et al., 1995; Andel et al., 1996). In Fig. 1 only one possibility is shown, the twofold isomerization around both the C_{15} single and the double bond from C_{15}-Z, *anti* in Pr (Fig. 1 *A*) to C_{15}-E, *syn* in Pfr (Fig. 1 *B*). It was suggested (Matysik et al., 1995; Andel et al., 1996) that Z-E (E-Z) isomerization takes place during the Pr→lumi-R (Pfr→lumi-F) transition, whereas C_{15} single bond rotation occurs in one of the subsequent steps.

Note that the reverse Pfr photoreaction is clearly faster than the forward Pr photoreaction. This observation holds equally for phytochrome of plants and for cyanobacterial phytochrome Cph1-PCB. In fact, the Pfr photoreaction is reminiscent of *trans-cis* photoisomerizations found in retinal proteins (Ottolenghi and Sheves, 1995, for review; Arlt et al., 1995; Lutz et al., 2000; Zinth et al., 2000). Both the low-fluorescence quantum yield (Sineshchekov et al., 1998) and the short time constants reported here indicate a barrier-free potential energy surface crossing between the excited state of Pfr and the photoproduct. In contrast, the Pr photoreaction is characterized by longer time constants and an activation barrier on the excited-state surface. The different shapes of the respective potential energy surfaces, especially the strong asymmetry with respect to the reaction rates, must be associated with distinct chromophore configurations and altered chromophore-protein interaction. Further experiments on modified chromophores, as for example, those on Cph1-PEB, and on mutants will elucidate the role of specific constituents in the chromophore binding pocket that might control the phytochrome reaction dynamics. Among them, local charges are expected to play an important role for the control of reaction rates as has been demonstrated in bacteriorhodopsin (Kobayashi et al., 1990; Song et al., 1993; Heyne et al., 2000).

This work was supported by the Deutsche Forschungsgemeinschaft (Sfb 450 (B3) and 498 (B2)).

REFERENCES

Andel, F., K. C. Hasson, F. Gui, P. A. Anfinrud, and R. A. Mathies. 1997. Femtosecond time-resolved spectroscopy of the primary photochemistry of phytochrome. *Biospectroscopy.* 3:421–431.

Andel, F., J. C. Lagarias, and R. A. Mathies. 1996. Resonance Raman analysis of chromophore structure in the lumi-R-photoproduct of phytochrome. *Biochemistry.* 35:15997–16008.

Arlt, T., S. Schmidt, W. Zinth, U. Haupts, and D. Oesterhelt. 1995. The initial reaction dynamics of the light-driven chloride pump halorhodopsin. *Chem. Phys. Lett.* 214:559–565.

Austin, R. H., K. W. Beeson, L. Eisenstein, H. Fraunfelder, and I. C. Gunsalus. 1975. Dynamics of ligand binding to myoglobin. *Biochemistry.* 14:5355–5373.

Bischoff, M. 2000. Femtosekundenspektroskopische Untersuchungen an Phytochromen. Ph.D. thesis. Friedrich-Schiller-Universität Jena and Biologisch-Pharmazeutische Fakultät, Jena, Germany. 1–110.

Bischoff, M., G. Hermann, S. Rentsch, and D. Strehlow. 2001. First steps in the phytochrome phototransformation: a comparative femtosecond study on the forward (Pr→Pfr) and back reaction (Pfr→Pr). *Biochemistry.* 40:181–186.

Bischoff, M., G. Hermann, S. Rentsch, and D. Strehlow. 1998. Ultrashort processes of native phytochrome: femtosecond kinetics of the far-red-absorbing form Pfr. *J. Phys. Chem. A.* 102:4399–4404.

Bischoff, M., G. Hermann, S. Rentsch, D. Strehlow, S. Winter, and H. Chosrowjan. 2000. Excited-state processes in phycocyanobilin studied by femtosecond spectroscopy. *J. Phys. Chem. B.* 104:1810–1816.

Braslavsky, S. E., J. I. Matthews, H. J. Herbert, J. de Kok, C. J. P. Spruit, and K. Schaffner. 1980. Characterization of a microsecond intermediate in the laser flash photolysis of small phytochrome from oat. *Photochem. Photobiol.* 31:417–426.

Büchler, R., G. Hermann, D. V. Lap, and S. Rentsch. 1995. Excited state relaxations of phytochrome studied by femtosecond spectroscopy. *Chem. Phys. Lett.* 233:514–518.

Casal, J. J., R. A. Sánchez, and J. F. Botto. 1998. Modes of action of phytochromes. *J. Exp. Bot.* 49:127–138.

Chory, J., M. Chatterjee, R. K. Cook, T. Elich, C. Frankhauser, J. Li, P. Nagpal, M. Neff, A. Pepper, D. Poole, J. Reed, and V. Vitart. 1996. From seed germination to flowering, light controls plant development via the pigment phytochrome. *Proc. Natl. Acad. Sci. U.S.A.* 93: 12066–12071.

Cordonnier, M. M., P. Mathis, and L. H. Pratt. 1981. Phototransformation kinetics of undegraded oat and pea phytochrome by laser flash excitation of the red absorbing form. *Photochem. Photobiol.* 34:733–740.

Eilfeld, P., and W. Rüdiger. 1985. Absorption spectra of phytochrome intermediates. *Z. Naturforsch.* 40C:109–114.

Foerstendorf, H., T. Lamparter, J. Hughes, W. Gärtner, and F. Siebert. 2000. The photoreactions of recombinant phytochrome from the cyanobacterium *Synechocystis*: a low temperature UV-Vis and FT-IR spectroscopic study. *Photochem. Photobiol.* 71:655–661.

Foerstendorf, H., E. Mummert, E. Schäfer, H. Scheer, and F. Siebert. 1996. Fourier-transform infrared spectroscopy of phytochrome. *Biochemistry.* 35:10793–10799.

Fraunfelder, H., and P. G. Wolynes. 1985. Rate theories and puzzles of hemeprotein kinetics. *Science.* 229:337–345.

Hermann, G., M. E. Lippitsch, H. Brunner, F. R. Aussenegg, and E. Müller. 1990. Picosecond dynamics of the excited state relaxations in phytochrome. *Photochem. Photobiol.* 52:13–18.

Heyne, K., J. Herbst, B. Dominguez-Herradon, U. Alexiev, and R. Diller. 2000. Reaction control in bacteriorhodopsin: impact of Arg82 and Asp85 on the fast retinal isomerization, studied in the second site revertant Arg82Ala/Gly231Cys and various purple and blue forms of bacteriorhodopsin. *J. Phys. Chem. B.* 104:6053–6058.

Holzwarth, A., E. Venuti, S. E. Braslavsky, and K. Schaffner. 1992. The phototransformation process in phytochrome. I. Ultrafast fluorescence component and kinetic models for the initial $P_r \rightarrow P_{fr}$ transformation steps in native phytochrome. *Biochim. Biophys. Acta.* 1140:59–68.

Holzwarth, A., J. Wendler, B. P. Ruzsicska, S. E. Braslavsky, and K. Schaffner. 1984. Picosecond time-resolved and stationary fluorescence of oat phytochrome highly enriched in the native 124 kDa protein. *Biochim. Biophys. Acta.* 791:265–273.

Hübschmann, T., T. Börner, E. Hartmann and T. Lamparter, 2001. Characterisation of the Cph1 holo-phytochrome from *Synechocystis* sp. PCC 6803. *Eur. J. Biochem.* 268:2055–2063.

Hughes, J., and T. Lamparter. 1999. Prokaryotes and phytochrome: the connection to chromophores and signaling. *Plant Physiol.* 121: 1059–1068.

Hughes, J., T. Lamparter, F. Mittmann, E. Hartmann, W. Gärtner, A. Wilde, and T. Börner. 1997. A procaryotic phytochrome. *Nature.* 386: 663.

Inoue, Y., W. Rüdiger, R. Grimm, and M. Furuya. 1990. The phototransformation pathway of dimeric oat phytochrome from the red-light-absorbing form to the far-red-light-absorbing form at physiological temperature is composed of four intermediates. *Photochem. Photobiol.* 52:1077–1083.

Kandori, H., K. Yoshihara, and S. Tokutomi. 1992. Primary processes of phytochrome: initial step of photomorphogenesis in green plants. *J. Am. Chem. Soc.* 114:10958–10959.

Kobayashi, T., M. Terauchi, T. Kouyama, M. Yoshizawa, and M. Taiji. 1990. Femtosecond spectroscopy of acidified and neutral bacteriorhodopsin. *In* SPIE Laser Applications in Life Sciences 1403. N. I. Koroteev and B.N. Toleutaev, editors. SPIE Bellingham, Washington, DC. 407–416.

Lamparter, T., B. Esteban, and J. Hughes. 2001. Phytochrome Cph1 from the cyanobacterium *Synechocystis* PCC6803: purification, assembly and quarternary structure. *Eur. J. Biochem.* 268:4720–4730.

Lamparter, T., F. Mittmann, W. Gärtner, T. Börner, E. Hartmann, and J. Hughes. 1997. Characterization of recombinant phytochrome from the cyanobacterium S*ynechocystis. Proc. Natl. Acad. Sci. U.S.A.* 94: 11792–11797.

Li, L., J. T. Murphy, and J. C. Lagarias. 1995. Continuous fluorescence assay of phytochrome assembly in vitro. *Biochemistry.* 34:7923–7930.

Lutz, I., A. Sieg, I. Boche, M. Otsuka, D. Oesterhelt, J. Wachtveitl, and W. Zinth. 2000. Primary reactions of sensory rhodopsins: two proteins with vastly different dynamics. *In* Ultrafast Phenomena, Vol. XII, Springer Series in Chemistry: Physics 66. T. Elsaesser, S. Mukamel, M. M. Murnane, and N. F. Scherer, editors. Springer, Berlin. 677–679.

Matysik, J., P. Hildebrandt, W. Schlamann, S. E. Braslavsky, and K. Schaffner. 1995. Fourier-transform resonance Raman spectroscopy of intermediates of the phytochrome photocycle. *Biochemistry.* 34: 10497–10509.

McWhirter, J. G., and E. R. Pike. 1978. On the numerical inversion of the Laplace transform and similar Fredholm integral equations of the first kind. *J. Phys. A Math. Gen.* 11:1729–1745.

Murphy, J. T., and J. C. Lagarias. 1997. The phytofluors: a new class of fluorescent protein probes. *Curr. Biol.* 7:870–876.

Ottolenghi, M., and M. Sheves. 1995. Photophysics and photochemistry of retinal proteins. *Isr. J. Chem.* 35:193–515.

Quail; P. H., M. T. Boylan, B. M. Parks, T. W. Short, Y. Xu, and D. Wagner. 1995. Phytochromes: photosensory perception and signal transduction. *Science.* 268:675–680.

Remberg, A. 1997. Helerologe Expression and Spektroskopische Charakterisierung rekombinanter Phytochrome aus *Avena sativa* und Synechocystos. Ph.D. thesis. Gerhard-Mercator-Universität Duisburg, Duisburg, Germany. 1–176.

Remberg, A., I. Lindner, T. Lamparter, J. Hughes, C. Kneip, P. Hildebrandt, S. E. Braslavsky, W. Gärtner, and K. Schaffner. 1997. Raman spectroscopic and light-induced kinetic characterization of a recombinant phytochrome of the cyanobacterium *Synechocystis*. *Biochemistry.* 36:13389–13396.

Rentsch, S., M. Bischoff, G. Hermann, and D. Strehlow. 1998. Fs spectroscopic studies of the plant photoreceptor phytochrome. *Appl. Phys. B.* 66:259–261.

Rentsch, S., G. Hermann, M. Bischoff, D. Strehlow, and M. Rentsch. 1997. Femtosecond spectroscopic studies on the red light-absorbing form of oat phytochrome and 2,3 dihydrobiliverdin. *Photochem. Photobiol.* 66: 585–590.

Rüdiger, W., F. Thümmler, E. Cmiel, and S. Schneider. 1983. Chromophore structure of the physiologically active form (P_{fr}) of phytochrome. *Proc. Natl. Acad. Sci. U.S.A.* 80:6244–6248.

Ruzsicska, B. P., S. E. Braslavsky, and K. Schaffner. 1985. The kinetics of the early stages of the phytochrome phototransformation $P_r \rightarrow P_{fr}$: a comparative study of small (60 kDa) and native (124 kDa) phytochromes from oat. *Photochem. Photobiol.* 41:681–688.

Savikhin, S., T. Wells, P.-S. Song, and W. S. Struve. 1993. Ultrafast pump-probe spectroscopy of native etiolated oat phytochrome. *Biochemistry.* 32:7512–7518.

Schaffner, K., S. E. Braslavsky, and A. R. Holzwarth. 1990. Photophysics and photochemistry of phytochrome. *In* Advances in Photochemistry, Vol. 15. D. H. Volman, G. S. Hammond, and K. Gollnik, editors. Wiley, New York. 229–277.

Schmidt, P., U. H. Westphal, K. Worm, S. E. Braslavsky, W. Gärtner, and K. Schaffner. 1996. Chromophore-protein interaction controls the complexity of the phytochrom photocycle. *J. Photochem. Photobiol. B.* 34:73–77.

Scurlock, R. D., S. E. Braslavsky, and K. Schaffner. 1993a. A phytochrome study using two-laser/two-color flash photolysis: I_{700} is a mandatory intermediate in the $P_r \rightarrow P_{fr}$ phototransformation. *Photochem. Photobiol.* 57:690–695.

Scurlock, R. D., C. Evans, S. E. Braslavsky, and K. Schaffner. 1993b. A phytochrome phototransformation study using two-laser/two-color flash photolysis: analysis of the decay mechanism of I_{700}. *Photochem. Photobiol.* 58:106–115.

Sineshchekov. V. A. 1995a. Evidence for the existence of two phytochrome A populations. *J. Photochem. Photobiol. B Biol.* 28:53–55.

Sineshchekov, V. A. 1995b. Photobiophysics and photobiochemistry of the heterogeneous phytochrome system. *Biochim. Biophys. Acta.* 1228: 125–164.

Sineshchekov, V., J. Hughes, E. Hartmann, and T. Lamparter. 1998. Fluorescence and photochemistry of recombinant phytochrome from the cyanobacterium *Synechocystis. Photochem. Photobiol.* 67:263–267.

Smith, H. 1999. Phytochromes: tripping the light fantastic. *Nature.* 400: 710–713.

Song, L., M. A. El-Sayed, and J. K. Lanyi. 1993. Protein catalysis of the retinal subpicosecond photoisomerization in the primary process of bacteriorhodopsin photosynthesis. *Science.* 261:891–894.

Spörlein, S., W. Zinth, and J. Wachtveitl. 1998. Vibrational coherence in photosynthetic reaction centers observed in the bacteriochlorophyll anion band. *J. Phys. Chem. B.* 102:7492–7496.

Thümmler, F., and W. Rüdiger. 1983. Models for the photoreversibility of phytochrome. *Tetrahedron.* 39:1943–1951.

van Thor, J. J., B. Borucki, W. Crielaard, H. Otto, T. Lamparter, J. Hughes, K. J. Hellingwerf, and M. P. Heyn. 2001. Light-induced proton release and proton uptake reactions in the cyanobacterial phytochrome Cph1. *Biochemistry.* In press.

Vos, M. H., C. Rischel, M. R. Jones, and J. L. Martin. 2000. Electrochromic detection of a coherent component in the formation of the charge pair P(+)H(L)(−) in bacterial reaction centers. *Biochemistry.* 39: 8353–8361.

Wang, Q., R. W. Schoenlein, L. A. Peteanu, R. A. Mathies, and C. V. Shank. 1994. Vibrationally coherent photochemistry in the femtosecond primary event of vision. *Science.* 266:422–424.

Wilhelm, T., J. Piel, and E. Riedle. 1997. Sub-20-fs pulses tunable across the visible from a blue pumped single pass noncollinear parametric converter. *Opt. Lett.* 22:1494–1496.

Ye, T., E. Gershgoren, N. Friedman, M. Ottolenghi, M. Sheves, and S. Ruhman. 1999. Resolving the primary dynamics of bacteriorhodopsin, and of a "C13═C14 locked" analog, in the reactive excited state. *Chem. Phys. Lett.* 314:429–434.

Yeh, K. C., S. H. Wu, J. T. Murphy, and J. C. Lagarias. 1997. A cyanobacterial phytochrome two-component light sensory system. *Science.* 277:1505–1508.

Zeidler, M., T. Lamparter, J. Hughes, E. Hartmann, A. Remberg, S. Braslavsky, K. Schaffner, and W. Gärtner. 1998. Recombinant phytochrome of the moss *Ceratodan purpureus*: heterologous expression and kinetic analysis of $P_r \rightarrow P_{fr}$ conversion. *Photochem. Photobiol.* 68: 857–863.

Zinth, W., A. Sieg, P. Huppmann, T. Blankenhorn, D. Oesterhelt, and M. Nonella. 2000. Femtosecond spectroscopy and model calculations for an understanding of the primary reaction in bacteriorhodopsin. *In* Ultrafast Phenomena, Vol. XII, Springer Series in Chemistry: Physics 66. T. Elsaesser, S. Mukamel, M. M. Murnane, and N. F. Scherer, editors. Springer, Berlin. 680–682.